Texture of Crystalline Solids
1979, Vol. 3, pp. 191-214

MICROPLASTICITY PREDICTIONS OF r-VALUES AND YIELD LOCI OF LOW CARBON SHEET STEELS DEFORMING BY <111> PENCIL GLIDE

S. L. SEMIATIN
Metalworking Section, Battelle Columbus Laboratories, Columbus, Ohio 43201

P. R. MORRIS
Research and Technology, Armco Inc., Middletown, Ohio 45043

and

H. R. PIEHLER
Carnegie-Mellon University, Pittsburgh, Pennsylvania 15213

(Received February 6, 1979)

Abstract: The plastic deformation of low carbon sheet steels has been analyzed using microplasticity models and Hill's theory of anisotropic continuum plasticity. The analytical methods used to determine the crystallite stress states which must be generated for the isostress (lower-bound) and isostrain (upper-bound) cases are briefly discussed and then applied to predict yield loci for three cold-rolled, annealed low-carbon steels (enameling iron, aluminum-killed steel, and interstitial-free steel) whose textures were characterized by crystallite orientation distribution functions. While measured r-values correlate best with upper-bound yield loci predictions for enameling iron, those for the aluminum-killed steels show better agreement with lower-bound yield loci predictions. In the case of the interstitial-free steel, measured r-values could not be accounted for by either upper- or lower-bound predictions. The yield loci measurements and predictions are reviewed in the context of Hill's continuum theory.

INTRODUCTION

Characterization of the plastic deformation of polycrystalline aggregates of metals requires a detailed knowledge of the operative mechanism of deformation of the individual crystallites, as well as a quantitative description of the preferred crystallographic orientation, or texture, which may be present. Although the deformation of the individual crystallites of an aggregate is usually inhomogeneous,[1] homogeneous flow by slip, twinning, or some other process is usually assumed in order to make analytical treatment tractable. Analysis of plastic deformation by slip has received the greatest attention,[2-6] perhaps because it is the most common room temperature deformation mechanism in metals of commercial interest. However, theoretical examination of other deformation modes as well as combinations of deformation modes can be found in the literature.[7,8]

Until recently, aggregate theories have been applied primarily for the prediction of plastic properties of isotropic materials.[4,9] The development of methods for the description of textures in terms of analytical distribution functions has facilitated modeling of real materials. The crystallite orientation distribution function (C.O.D.F.),[10-13] derivable from standard pole figure data, unambiguously defines the probability of finding a crystallite at a specified orientation relative to fixed specimen axes. Three Eulerian angles are used in this specification, unlike the two angles which are used in plotting pole figures in the plane of a stereographic projection. Thus a three-dimensional representation or a series of two-dimensional sections are needed to represent the C.O.D.F.

The prediction of deformation textures and r-values of low-carbon steels have been among the first problems to be addressed using aggregate theory in conjunction with measured C.O.D.F.'s. Dillamore and Katoh[14] have examined the textures developed in heavily cold-rolled iron samples and found that upper-bound theories, such as that of Taylor,[15] yield results in closer agreement with measurement than lower-bound estimates derived from a Sachs type approach.[2] Parnière and his coworkers[16,17] have also used the Taylor theory[15] in order to estimate such plastic properties as r-values. Although their predictions of the average plastic strain ratio, $\bar{r}$, of an aluminum-killed steel agreed closely with measured values, deviations of up to 25% from measurements of r along certain directions could be noted.

The objective of the present paper is to describe briefly some methods for deriving upper-bound yield loci as well as lower-bound yield loci whose characteristics can be easily verified experimentally. Among these characteristics are the plastic strain ratio (r-value) and the ratio of the plane-strain flow stress to the uniaxial flow stress. Predictions and measurements for low-carbon steels of varying degrees of anisotropy will be described to illustrate the applicability of the upper- and lower-bound models to materials which deform by <111> pencil glide.[18]

DERIVATION OF YIELD LOCI

The yielding and plastic flow of three cold-rolled, annealed low-carbon steel sheets under states of plane stress have been studied. These materials exhibit three mirror planes of symmetry (one perpendicular to the sheet and containing the rolling direction, one perpendicular to the sheet and containing the transverse direction, and the midplane of the sheet). With this type of orthotropic symmetry, variations of the yield loci (σ_y vs. σ_x) in the plane of the sheet may be expected as the coordinate axes x, y are rotated about the sheet normal (see Figure 1). The plastic strain ratio, $d\varepsilon_y/d\varepsilon_z$, or r-value, for stress states consisting of uniaxial tension along x will also show a planar anisotropy.

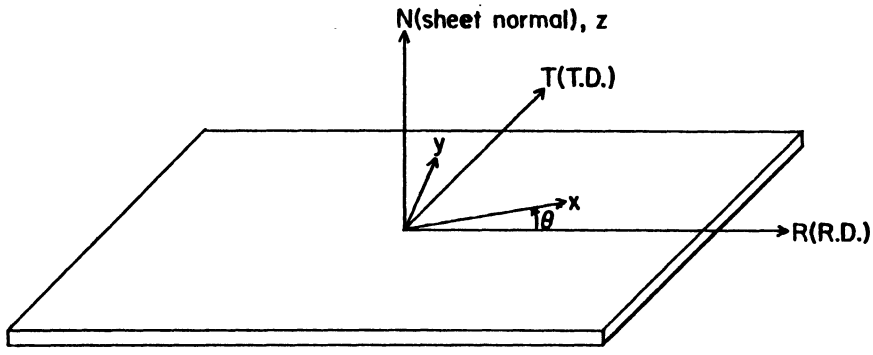

Figure 1. Coordinate axis systems of rolled sheet metals.

The stresses and strains referred to the coordinate x, y axes will vary from one crystallite to another. Furthermore, the principal axes of stress of the aggregate will not necessarily coincide with the principal axes of strain. However, bounds on the expected yielding behavior of the aggregate may be obtained by assuming all crystallites to experience the same strain state (isostrain or upper-bound model) or the same stress ratio (isostress or lower-bound model).[19] For both cases, plane-stress yield loci were found by setting $\sigma_z = 0$, and deformation was assumed to occur by <111> pencil glide.

Upper-Bound Yield Locus Determination

If each crystallite of the aggregate is assumed to experience the same strain state, the yield locus will be an upper bound to the actual behavior. For simplicity, consideration will be focused on deformations which give rise to the principal strains $d\varepsilon_x$, $d\varepsilon_y$, and $d\varepsilon_z$ along the coordinate x, y, z axes (Figure 1). When these strains are imposed, normal as well as shear stresses will be generated in the x, y, z system. These shear stresses for a sheet with orthotropic physical symmetry will be limited to the stress τ_{xy}.

To determine that stress state in each crystallite which can bring about yielding to accommodate the specified strain, the procedure developed by Morris and Semiatin[6] for deformation by <111> pencil glide has been employed for low-carbon

steels. Imposing an arbitrary strain requires the activation of either 3 or all 4 of the <111> pencil glide systems. A basic assumption of the procedure is that slip is governed by a critical resolved shear stress (CRSS) law, i.e., slip occurs when the shear stress reaches a value of K on the slip plane in the slip direction. This CRSS is assumed to be the same for all slip systems. Hence, the analysis is strictly valid only for predictions of yielding at small strains for which differential work hardening among the slip systems is negligible.

Once the shears and slip-plane orientations which accommodate the strain have been selected, the required stresses referred to the cubic-crystal axes and thus the x, y, z axes can be determined. The stress state referred to the crystal axes will in general involve shear stresses as well as terms comprised of differences of normal stresses (Bishop and Hill stresses[4]). This apparent ambiguity is resolved by adjusting the hydrostatic pressure, or, in the present case, by setting σ_z equal to zero. Averaging the stresses referred to the x, y, z axes over all crystallites gives one point on the upper-bound yield locus. Note that the upper-bound yield locus (or planar-strain yield locus, using Piehler and Backofen's terminology[19]) depicts only those normal stresses σ_x and σ_y associated with the principal strains $d\varepsilon_x$ and $d\varepsilon_y$. Information about the shear stresses which may be generated is not displayed in this presentation.

An entire upper-bound yield locus can be calculated by examining different principal strain states ($d\varepsilon_x$, $d\varepsilon_y$, $d\varepsilon_z$) along the principal strain axes x, y, z. Two important data points on the yield locus are (i) the stress state for which $d\varepsilon_y$ is equal to zero (the plane-strain flow stress[20]) and (ii) the stress state which corresponds to uniaxial tension, $\sigma_x = \sigma_u$, $\sigma_y = 0$. The latter is more difficult to determine since the specified strain state must be varied until the desired stress state ($\sigma_y = 0$) is found. When this strain state is found, the r-value is simply $d\varepsilon_y/d\varepsilon_z$.

An alternative procedure for determining the upper-bound yield locus of a single crystal or polycrystalline aggregate may be derived by making use of the theorem of virtual work.[4] The procedure will first be described for a single crystal. Denoting the single crystal normal stresses in the x, y, z system by σ_x^s and σ_y^s, the external work done by these stresses through the strains $d\varepsilon_x$, $d\varepsilon_y$, $d\varepsilon_z$ must be equal to the internal work done in producing the shears, γ, on the active slip planes, $K\Sigma|\gamma|$, the summation taken over all slip systems:

$$\sigma_x^s d\varepsilon_x + \sigma_y^s d\varepsilon_y = K\Sigma|\gamma| \quad , \tag{1}$$

or

$$\sigma_x^s/K + (\sigma_y^s/K)d\varepsilon_y/d\varepsilon_x = (\Sigma|\gamma|)/d\varepsilon_x \quad . \tag{2}$$

The factor $(\Sigma|\gamma|)/d\varepsilon_x$ is called the Taylor factor and denoted by M. Defining $Q = -d\varepsilon_y/d\varepsilon_x$ and taking d/dQ of Eq. (2) results in

$$\frac{d}{dQ}(\sigma_x^s/K) - Q\frac{d}{dQ}(\sigma_y^s/K) - \frac{\sigma_y^s}{K} = \frac{dM}{dQ} \quad . \tag{3}$$

From the normality condition,[21]

$$\frac{d\sigma_y^s}{d\sigma_x^s} = -\frac{d\varepsilon_x}{d\varepsilon_y} = \frac{1}{Q} \ ,$$

we obtain

$$Q\frac{d(\sigma_y^s/K)}{dQ} = \frac{d(\sigma_x^s/K)}{dQ} \ ,$$

and Eq. (3) becomes

$$\frac{\sigma_y^s}{K} = -\frac{dM}{dQ} \quad . \tag{4}$$

Equations (2) and (4) can be used to obtain σ_x^s,

$$\frac{\sigma_x^s}{K} = M - Q\frac{dM}{dQ} \quad . \tag{5}$$

Since a relation of the form of Eq. (1) must hold for each crystallite of the aggregate, Eqs. (4) and (5) may be generalized for the aggregate,

$$\frac{\sigma_y}{K} = -\frac{d\bar{M}}{dQ} \ , \tag{6}$$

and

$$\frac{\sigma_x}{K} = \bar{M}(Q) - Q\frac{d\bar{M}(Q)}{dQ} \quad . \tag{7}$$

$\bar{M}$ is the average M value of the aggregate as a function of Q. When $d\bar{M}/dQ$ is equal to zero (e.g., when M passes through a minimum), $\sigma_y/K = 0$. This corresponds to uniaxial tension, and from Eq. (7), $\sigma_x/K = \bar{M}$.[22] The r-value is easily determined from the Q value, $r = Q/(1-Q)$ (Figure 2). For $Q = 0$ (plane strain), $\sigma_x/K = \bar{M}$ also.

Using Eqs. (6) and (7), the entire upper-bound yield locus can be generated from a plot of $\bar{M}$ vs. Q. Deriving the yield locus in this manner requires less labor than the first technique which involves the added calculations of the stress transformations from the cubic axes to the principal axes of strain. On the other hand, for moderately textured materials, the former method is to be preferred when accurate determination of the yield locus close to $\sigma_y = 0$ is desired since the $\bar{M}$ vs. Q curve is usually fairly flat near the minimum.

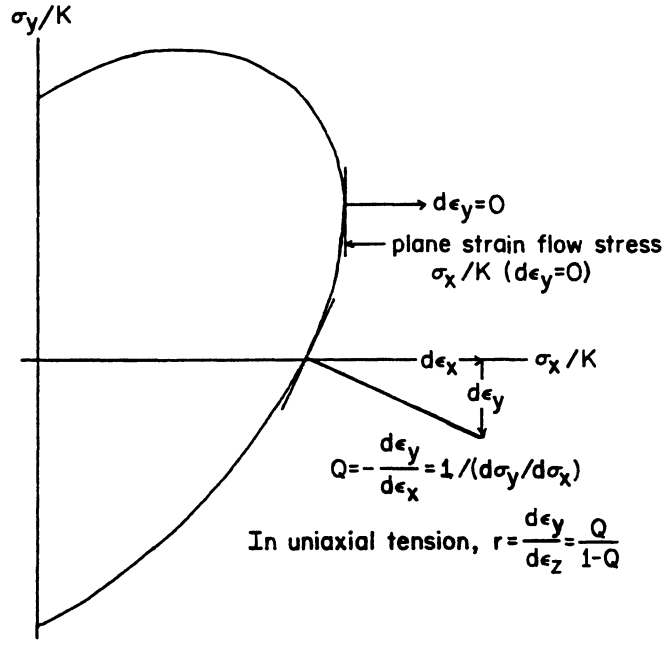

Figure 2. Determination of r-value and plane-strain flow stress from yield locus.

Lower-Bound Yield Locus Determination

The lower-bound yield locus of low-carbon steels can be derived using techniques developed by Piehler and Backofen.[5,19] In this case it is assumed that the x, y, z axes (Figure 1) are the principal axes of stress of the aggregate, and that all crystallites experience the same imposed stress ratio ($\sigma_y:\sigma_x = \alpha$, $\sigma_z = 0$). For each α, the pencil glide slip system which has the greatest resolved shear stress acting on it is found for each crystallite using the relations in Table II of Ref. 5. It is postulated that the crystallite yields when the CRSS, K, is reached on that slip system. In general, varying levels of σ_y and σ_x must be applied for crystals of different orientations to bring about yielding, even though the ratio σ_y/σ_x is the same for all. As Piehler and Backofen[19] have noted, the yield locus obtained by averaging σ_y and σ_x at the same stress ratio is a lower bound only in an average sense.

By examining different stress ratios, the lower-bound, or, in Piehler and Backofen's terminology, planar-stress, yield locus can be calculated for a polycrystalline aggregate. Again, the properties of primary interest will be the plastic strain ratio (r-value) and the ratio of the plane-strain flow stress to the uniaxial flow stress. The r-value is determined from the slope of the yield locus at $\sigma_y = 0$, and the plane-strain flow stress is the stress σ_x at the farthest extent of the yield locus into the first quadrant (see Figure 2).

Permissible Range of r-Values

The r-values which correspond to the upper- and lower-bound yield loci do not necessarily form bounds to the actual r-value. It is, however, possible to calculate *permissible* ranges of r-values from upper- and lower-bound yield loci. This procedure will be illustrated with reference to Figure 3, which contains upper and lower bounds to the yield locus for a sheet composed of a "cube-on-face" texture, i.e.,

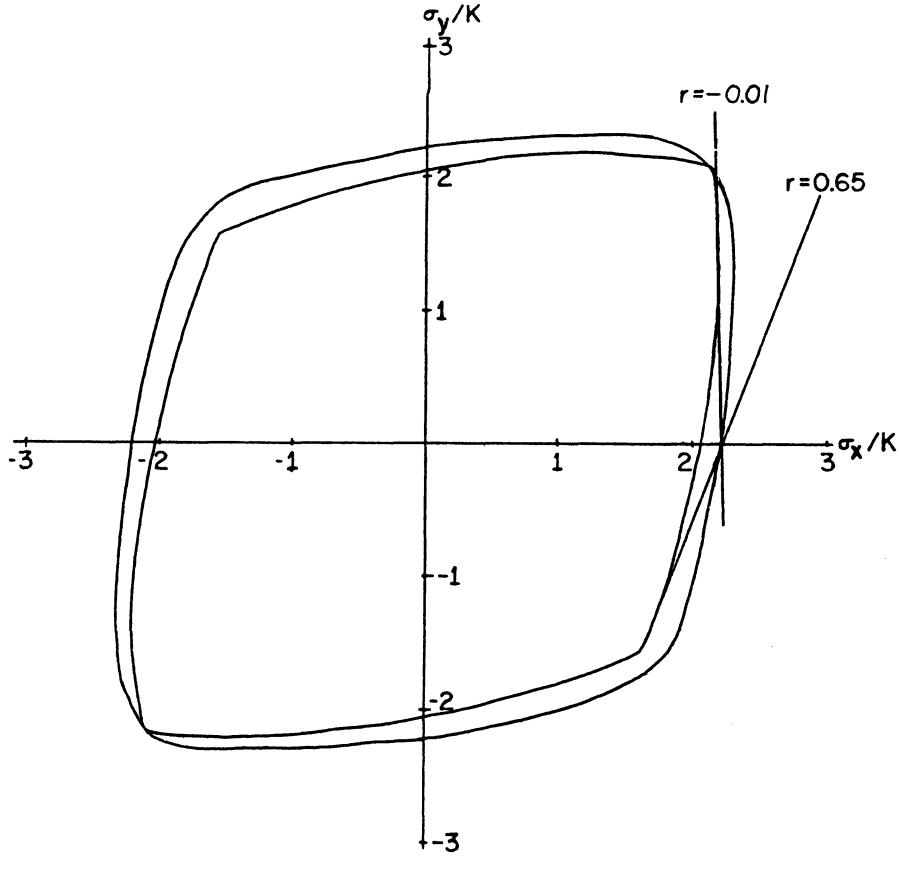

Figure 3. Lower- and upper-bound yield loci for rotationally-symmetric cube-on-face texture, pencil glide.

<100> parallel to N, Figure 1. These pencil-glide yield loci are for a cube-on-face texture which is rotationally symmetric about the sheet normal, and are similar in shape to the loci which were calculated assuming deformation by restricted glide (<111>{111} slip).[19] The *lowest* r-value is obtained from the most nearly vertical slope at the σ_x/K axis of a permissible yield locus between the upper and lower bounds. (A vertical yield locus at the σ_x/K axis corresponds to plane strain or r = 0). The *highest* r-value is obtained from the slope at the σ_x/K axis of a permissible yield locus between the upper and lower bounds which is most nearly equal to 45°.

(A 45° slope corresponds to r = ∞.) The graphically determined minimum and maximum r-values are r_{min} = -0.01 (a physically disturbing result), and r_{max} = 0.65. These may be compared with r = 0.30 calculated from the slope of the lower-bound yield locus and r = 0.10 calculated from the slope of the upper-bound yield locus, both measured at the σ_x/K axis.

This procedure is very tedious and, due to its graphical nature, subject to substantial errors. It has not been used in the remainder of the study, since it was found that many of the trends to be discussed can be explained on the basis of r-values predicted directly from the slopes of the upper- and lower-bound yield loci themselves.

MATERIALS AND PROCEDURE

Three cold-rolled, annealed low-carbon steels with a wide range of $\bar{r}$-values were selected for experimental investigation and comparison with aggregate-theory calculations. All had a nominal thickness of 1.0 mm (0.040 in). An enameling iron (nominal composition <0.02% C) was chosen to represent a fairly isotropic material with $\bar{r} \approx 1.0$. A drawing-quality, aluminum-killed steel (0.047% C, 0.33% Mn, 0.058% Al) with an $\bar{r}$ of 1.6 represented a steel of intermediate drawing quality obtainable by commercial processing. Lastly, an interstitial-free steel (0.011% C, 0.18% Mn, 0.055% Al, 0.067% Cb, 0.056% Ti) with an $\bar{r}$ = 2.0 was used. All steels had an ASTM grain size between 7 and 8.

The r-values of the materials were measured in two ways. The simpler method consisted of straining tensile samples to approximately 18% elongation and measuring the distances between two pairs of gage marks, one along the tensile axis and the other along the width direction. Each pair was originally 19.05 mm (0.750 in) apart. From these measurements, the width strain and thickness strain could be calculated (using the constant-volume assumption), and the r-value taken to be the ratio of the two. Alternatively, tensile samples were strained, and width measurements taken with a micrometer at extension increments of 5%. From these data, plots of ε_w versus ε_t were obtained, and the r-value was taken as the slope of the best straight line fit. The two methods gave r-values within ±0.10 of each other, and this number can be taken to be the reliability of the r-value measurements as well. These experimental measurements were made at 10° increments between the rolling and transverse directions for the aluminum-killed steel. Because of material limitations, however, measurements only at 0° (R.D.), 45° to the R.D., and 90° to the R.D. (T.D.) were obtained for the enameling iron and the interstitial-free steel.

The textures of the materials were characterized using an Enraf-Nonius single-crystal diffractometer. Three reflection X-ray pole figures (110, 200, and 211) were measured for each steel. Use of composite sampling techniques[2,3] allowed the averaging of texture gradients which may have existed through the thickness. From the measured pole figure data, the coefficients of a 16th order crystallite orientation distribution function (C.O.D.F.) were derived.[13] The textures

could then be described. Selecting a mesh size of 6° x 6° x 6° in the Eulerian octant $0 \leq \psi \leq \pi/2$, $0 \leq \theta \leq \pi/2$, $0 \leq \phi \leq \pi/2$, the probabilities (times random) of finding crystallites at orientations uniformly distributed over the angles ψ, θ, and ϕ were determined from the C.O.D.F. The boundary data points were chosen to be 3° away from $\psi = 0, \pi/2$, $\theta = 0, \pi/2$, and $\phi = 0, \pi/2$, and, therefore, there were $15^3 = 3375$ mesh points in the octant. For the plane-stress problems under consideration, two Eulerian octants ($0 \leq \psi \leq \pi/2$, $0 \leq \theta \leq \pi/2$, $0 \leq \phi \leq \pi/2$ and $0 \leq -\psi \leq \pi/2$, $0 \leq \theta \leq \pi/2$, $0 \leq -\phi \leq \pi/2$) had to be used to enforce orthotropic physical symmetry. The probabilities at corresponding points in the two octants were taken to be equal.

The total number of crystallite calculations to find one point on the upper-bound or lower-bound yield loci was 3375 x 2 = 6750. Using the formulation of Morris and Semiatin,[6] the calculation of one point on the isostrain or upper-bound yield locus using a Modcomp computer took approximately 14 minutes of execution time. The simpler lower-bound program used approximately 40 seconds. In both cases, data were accessed from disk storage. In addition, several runs were made on an IBM 370 computer, and it was found that execution time could be reduced by a factor of 12 by using this system.

For the more highly textured steels (i.e., aluminum-killed and interstitial-free steels), the curve fitting process entailed in obtaining the C.O.D.F. resulted in negative probabilities of finding crystallites in certain orientations. These negative probabilities are an artifact created by the series solution process. Although runs were made both with and without orientations of negative probability included, the results reported here are for cases where they have been excluded. It is thought that these cases model the physics of the problem more closely. Moreover, model predictions for the less highly oriented materials are more reliable, since the texture description is probably more accurate.

In both upper- and lower-bound programs, the primary data which were averaged over all crystallites were the stresses referred to either the principal axes of strain (upper-bound program) or principal axes of stress (lower-bound program). The following relation was used for averaging

$$\sigma_{av.} = \frac{\iiint \sigma(\psi,\theta,\phi) w(\psi,\theta,\phi) \sin\theta \, d\psi d\theta d\phi}{\iiint w(\psi,\theta,\phi) \sin\theta \, d\psi d\theta d\phi} \quad . \tag{8}$$

In this relation, w is the probability of finding a crystallite with an orientation specified by the Eulerian angles ψ,θ,ϕ. The integrations are carried out over the two Eulerian octants. For further details on the mechanics of determining C.O.D.F.'s and their use, the reader may consult Ref. 13.

The r-values from the upper-bound yield locus were found by an iterative procedure in which the imposed strain state specified by Q ($= -d\varepsilon_y/d\varepsilon_x$) was varied until $|\sigma_y/K|$ of the aggregate was equal to or less than 0.001. To obtain the desired convergence, between 5 and 15 iterations were needed for a starting Q of 0.00 (i.e., plane strain). Lower-bound yield locus r-values were predicted by determining the

aggregate stress states for $\alpha = 0.01$ and $\alpha = -0.01$. Application of the normality condition to this section of the yield locus gave the r-value immediately.

The reproducibility of r-value predictions was determined by calculating r-values from two sets of C.O.D.F. measurements on samples from the same lot of the aluminum-killed steel. In all cases the r-values along any given direction were within ±0.10 of each other.

RESULTS AND DISCUSSION

r-Values

Plots of measured r-values and r-values predicted from the upper- and lower-bound yield loci for the three low-carbon steels are given in Figures 4-6. In addition, $\bar{r} = (r_{0°} + 2r_{45°} + r_{90°})/4$ and $\Delta r = (r_{0°} - 2r_{45°} + r_{90°})/2$ are summarized in Table I. The prediction of r-values from the

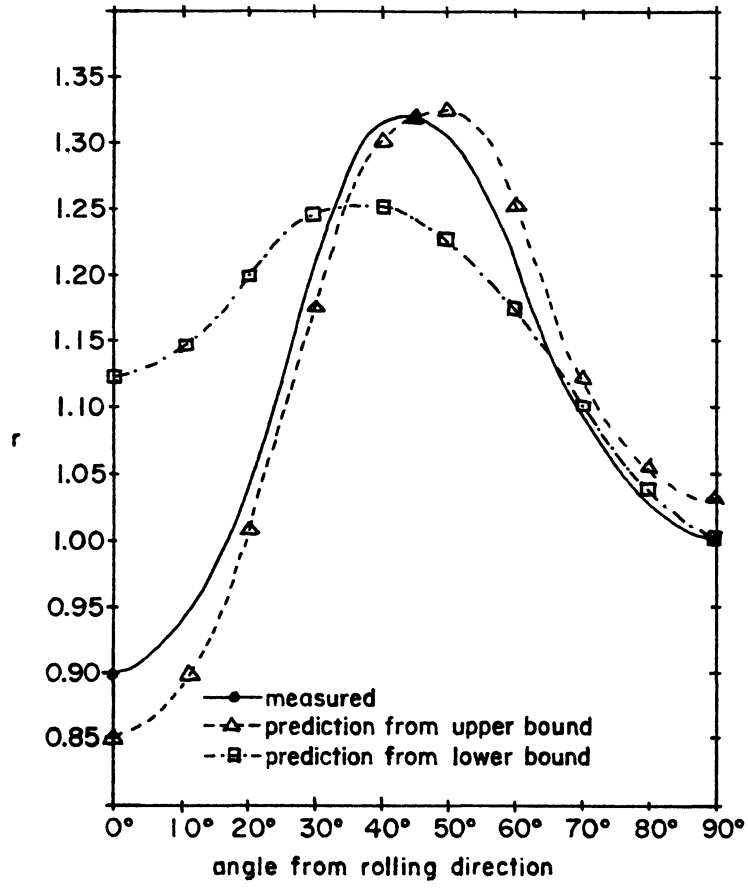

Figure 4. Measured and predicted r-values versus angle from the rolling direction for enameling iron.

TABLE I

MEASURED AND PREDICTED $\bar{r}$-VALUES AND Δr's OF LOW CARBON STEELS

Steel	Measured $\bar{r}$	Measured Δr	Texture Sample	Predicted $\bar{r}$, Lower-Bound Yield Locus	Predicted Δr, Lower-Bound Yield Locus	Predicted $\bar{r}$, Upper-Bound Yield Locus	Predicted Δr, Upper-Bound Yield Locus
Enameling iron	1.14	-0.37	Composite	1.15	-0.18	1.13	-0.38
Aluminum-killed steel	1.62	0.74	Composite	1.66	0.52	1.97	1.03
Interstitial-free steel	1.96	-0.13	Composite	1.80	0.16	2.13	0.27
Aluminum-killed steel	1.62	0.74	Midplane	1.64	0.33	1.84	0.61

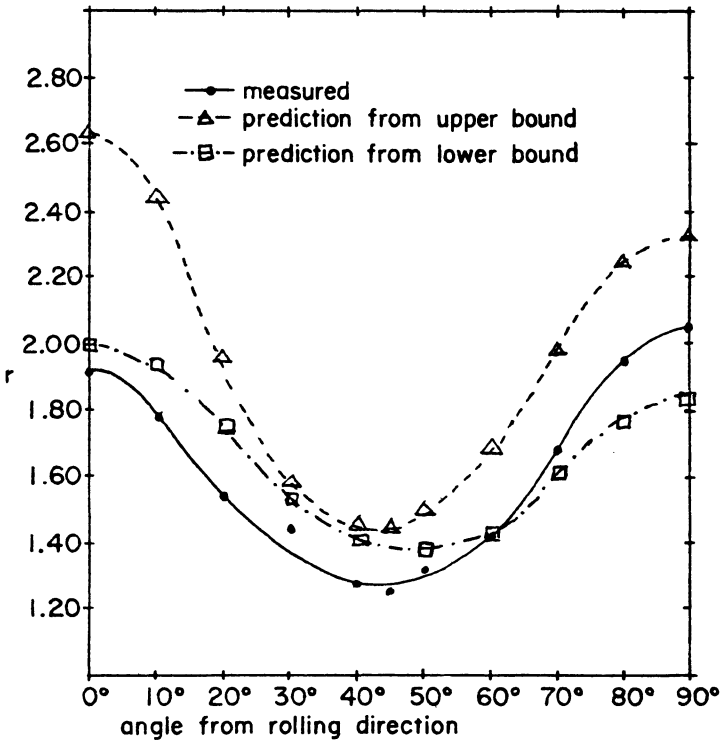

Figure 5. Measured and predicted r-values versus angle from the rolling direction for aluminum-killed steel.

upper-bound yield locus shows excellent agreement with measurements for the weakly textured enameling iron (Figure 4). Lower-bound yield locus predictions for this material also agree reasonably well with measured values, especially when only r-values and Δr values are compared (Table I).

A different trend can be noticed upon examination of the data for the more highly-textured materials, aluminum-killed steel and the interstitial-free, low-carbon steel (Figures 5 and 6). In contrast to the enameling iron results for which better agreement was obtained using the upper-bound yield locus, isostress, or lower-bound, yield locus r-value predictions are closer to measured values for the aluminum-killed steel. Neither upper- nor lower-bound yield loci r-value predictions appear to follow the measured pattern for the interstitial-free steel (Figure 6). It is believed that this discrepancy exists because the 16th order C.O.D.F. fit used is not accurate enough for this sharply-textured material.[24] However, the measured $\bar{r}$ for this material is indeed bounded by the $\bar{r}$'s of the two models, even if the Δr is not (Table I).

The possible influence of through-thickness texture gradients on r-value predictions was investigated for the aluminum-killed steel. Yield loci and r-value calculations were carried out for a C.O.D.F. derived from reflection pole figure data obtained for the midplane of sheet samples. A program

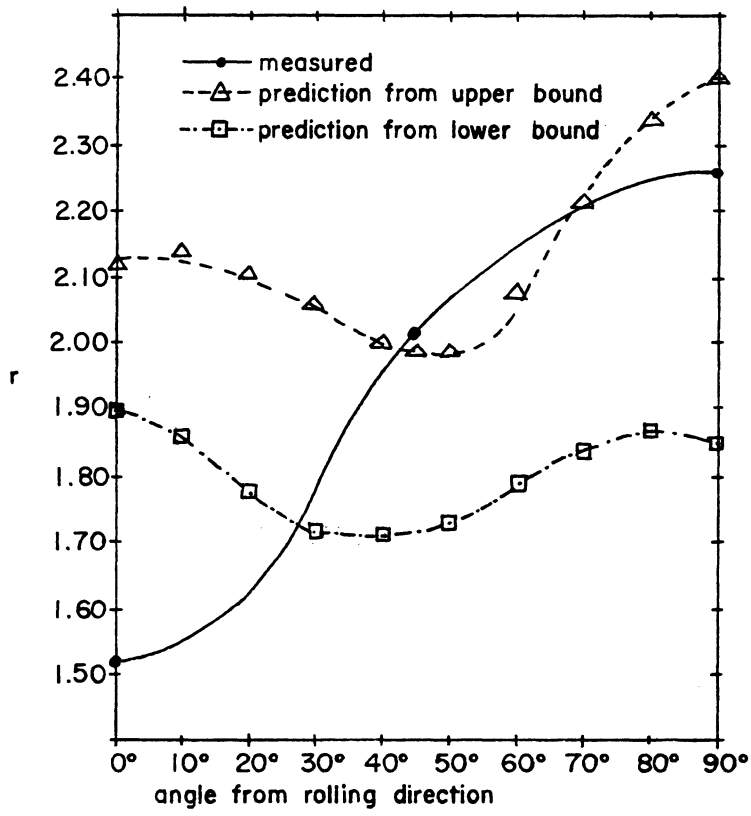

Figure 6. Measured and predicted r-values versus angle from rolling direction for interstitial-free steel.

which gave a 22nd order polynomial fit for the C.O.D.F. was available for this purpose. In Figure 7, r-value predictions from these texture data are plotted. Although the lower-bound yield locus predictions are relatively unchanged, the comparison between the upper-bound yield locus predictions and measured values is substantially improved (Figure 7 and Table I). This may be partially due to improved texture data from the 22nd order fit. It must also not be overlooked that the textural "contribution" of surface grains (which are less constrained and less apt to conform to isostrain deformation imposed by their neighbors) has been eliminated. For this steel, as well as the others, there are approximately 35 grains across the thickness. Therefore, regions for which isostress and isostrain deformation occur may be comparable, and the use of midplane texture data in the isostrain analysis may be more appropriate than the composite sample data.

The presence of microtexture (crystallites which are likely to have nearest neighbors of similar orientation) may explain the different behavior exhibited by enameling iron and aluminum-killed steel. For the mildly textured enameling iron, the intensity peaks of the C.O.D.F. were on the order of 2-3 times random. For the killed steel, these peaks

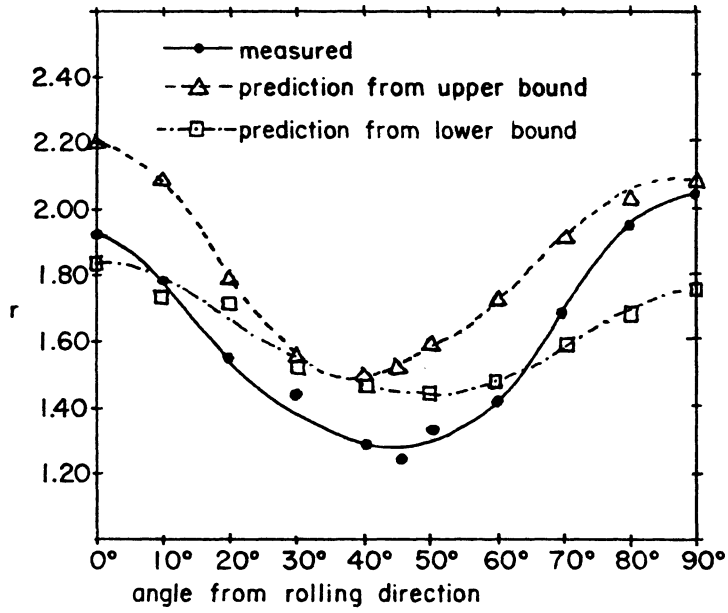

Figure 7. Measured and predicted r-values versus angle from rolling direction for aluminum-killed steel (midplane texture measurements used for predictions).

were on the order of 5-6 times random. These differences are typical of rimmed and aluminum-killed cold-rolled, annealed low-carbon steels.[25] Hence, it is reasonable to assume that crystallites with nearest neighbors of similar orientation are more likely to be found in the killed steel than in the rimmed steel (enameling iron). When nearest neighbors are of similar orientation, deformation is probably easy to accommodate by the activation of only one or two slip systems. In this case, isostress behavior is more plausible than when constraints are increased and polyslip required to occur. This explains why the r-values of the killed steel are better predicted by the isostress model (Figure 5) and why the less-textured enameling iron seems to follow the isostrain model. It appears that microtexture plays a similar role in determining the applicability of upper- and lower-bound models for prediction of the elastic constants of highly-texture steels.[26] Further evidence to support these conclusions will now be presented.

Yield Loci Predictions from Aggregate Theory

The applicability of the isostress or isostrain hypotheses for the description of low-carbon steel yield loci was examined using the ratio of the plane-strain flow stress, $\sigma_{1(0)}$, to the uniaxial flow stress, σ_u. Again, the upper- and lower-bound yield loci cannot be expected to provide bounds for this ratio, but useful insights have been gained from these yield loci. Predictions from the upper- and lower-bound yield loci are given in Table II. Note that the stresses, $\sigma_{1(0)}$ and σ_u,

TABLE II

YIELD-LOCUS MODEL PREDICTIONS

Material	Upper-Bound Yield-Locus Predictions				Lower-Bound Yield-Locus Predictions			
	r	σ_u/K	$\sigma_{l(0)}/K$	$\sigma_{l(0)}/\sigma_u$	r	σ_u/K	$\sigma_{l(0)}/K$	$\sigma_{l(0)}/\sigma_u$
Isotropic Aggregate	1.00	2.739	3.066	1.119	1.00	2.121	2.466	1.163
Enameling Iron (composite sample)								
0° to R.D.	0.85	2.826	3.086	1.092	1.12	2.077	2.470	1.189
45° to R.D.	1.32	2.714	3.129	1.153	1.24	2.111	2.501	1.185
90° to R.D.	1.03	2.806	3.109	1.108	1.00	2.129	2.511	1.180
Aluminum-Killed Steel (composite sample)								
0° to R.D.	2.64	2.745	3.294	1.200	1.99	2.081	2.616	1.257
45° to R.D.	1.46	2.857	3.288	1.151	1.40	2.138	2.590	1.211
90° to R.D.	2.33	2.722	3.278	1.204	1.84	2.117	2.626	1.240
Aluminum-Killed Steel (midplane sample)								
0° to R.D.	2.20	2.780	3.257	1.172	1.85	2.080	2.588	1.244
45° to R.D.	1.53	2.825	3.270	1.158	1.47	2.126	2.587	1.217
90° to R.D.	2.08	2.760	3.275	1.187	1.75	2.123	2.631	1.240

have been normalized by the critical resolved shear stress, K. Because of grain size effects, among other things, the actual values of $\sigma_{1(0)}/K$ and σ_u/K are probably not very accurate. The ratio $\sigma_{1(0)}/\sigma_u$ is perhaps more reliable since these effects probably influence all stress states proportionately.

Model predictions for an isotropic aggregate of BCC crystallites (Table II) differ somewhat from continuum-mechanics predictions such as those of the von Mises criterion. Whereas a $\sigma_{1(0)}/\sigma_u$ of 1.119 (upper-bound model) is below the von Mises prediction of 1.155, the lower-bound yield locus prediction, 1.163, exceeds it. This upper-bound prediction is close to that of 1.122 from Hutchinson's "approximate" pencil-glide analysis.[9] For FCC metals which deform by <110>{111} restricted slip, Bishop and Hill's upper-bound analysis[4] for an isotropic aggregate predicts a $\sigma_{1(0)}/\sigma_u$ of 1.079, also somewhat below the von Mises value. For all the low-carbon sheet steels investigated, lower-bound yield locus predictions of $\sigma_{1(0)}/\sigma_u$ exceed upper-bound yield locus predictions (Table II). These results and several experimental measurements will next be discussed in the context of Hill's anisotropic continuum-plasticity theory.[27]

Hill's Continuum Theory

Hill's generalization of the von Mises yield criterion for plastically anisotropic materials with orthotropic physical symmetry deformed in plane stress can be written:

$$F\sigma_{yy}^2 + G\sigma_{xx}^2 + H(\sigma_{xx} - \sigma_{yy})^2 + 2N\tau_{xy}^2 = 1. \qquad (9)$$

The stresses σ_{xx}, σ_{yy}, and τ_{xy} are stresses referred to the principal axes of anisotropy, which, for rolled sheet materials are the rolling, transverse, and sheet-normal directions (Figure 1). The flow rule associated with Eq. (9) is:

$$\left.\begin{aligned} d\varepsilon_{xx} &= d\lambda[H(\sigma_{xx} - \sigma_{yy}) + G\sigma_{xx}] \\ d\varepsilon_{yy} &= d\lambda[H(\sigma_{yy} - \sigma_{xx}) + F\sigma_{yy}] \\ d\varepsilon_{zz} &= -d\varepsilon_{xx} - d\varepsilon_{yy} = d\lambda[-G\sigma_{xx} - F\sigma_{yy}] \\ d\varepsilon_{xy} &= d\lambda[N\tau_{xy}] \end{aligned}\right\} \qquad (10)$$

($d\lambda$ = proportionality constant)

Using Eqs. (9) and (10), three of the constants F, G, H, and N can be expressed as functions of the fourth and the r-values corresponding to tensile tests along three directions. Typically, the rolling direction, transverse direction, and diagonal r-values ($r_{0°}$, $r_{45°}$, and $r_{90°}$) are employed[28] with the results:

$$G = H/r_{0°} ,$$

$$F = H/r_{90°}, \text{ and} \tag{11}$$

$$N = (H/r_{0°})\left(r_{45°} + \frac{1}{2}\right)\left(1 + \frac{r_{0°}}{r_{90°}}\right) .$$

For a tensile test along the rolling direction ($\sigma_{yy} = \tau_{xy} = 0$), Eqs. (9) and (11) give

$$\sigma_u|_{0°} = (G + H)^{-\frac{1}{2}} = F^{-\frac{1}{2}}\,[r_{90°} + (r_{90°}/r_{0°})]^{-\frac{1}{2}} . \tag{12}$$

Equations (10) can be used to obtain σ_{yy} for a plane strain extension along the rolling direction ($d\varepsilon_{yy} = d\varepsilon_{xy} = 0$),

$$\sigma_{yy} = \sigma_{xx}/[1 + (F/H)],$$

and the yield condition Eq. (9) can be applied to obtain the plane-strain yield stress:

$$\sigma_{1(0)}|_{0°} = F^{-\frac{1}{2}}\left(\frac{r_{90°}}{1 + r_{90°}} + \frac{r_{90°}}{r_{0°}}\right)^{-\frac{1}{2}} . \tag{13}$$

Dividing Eq. (13) by Eq. (12) gives an expression for $\sigma_{1(0)}/\sigma_u$

$$\left.\frac{\sigma_{1(0)}}{\sigma_u}\right|_{0°} = \left\{\frac{(1 + r_{0°})(1 + r_{90°})}{1 + r_{0°} + r_{90°}}\right\}^{\frac{1}{2}} . \tag{14}$$

Surprisingly, the result, Eq. (14), is identical for $(\sigma_{1(0)}/\sigma_u)|_{90°}$. It can be noted that this result contains only the r-values for 0° and 90°. Furthermore, when the anisotropy is rotationally symmetric about the sheet normal (i.e., for planar isotropy, $r_{0°} = r_{45°} = r_{90°} = r_\theta = R$), Eq. (14) reduces to the familiar form[29]

$$\frac{\sigma_{1(0)}}{\sigma_u} = \frac{1 + R}{\sqrt{1 + 2R}} . \tag{15}$$

Comparison of Aggregate- and Continuum-Theory Yield-Loci Predictions

Aggregate theory predictions can now be compared with those from Hill's continuum plasticity theory. Model predictions are summarized in Table III for both enameling iron and the aluminum-killed steel. Hill predictions of $\sigma_{1(0)}/\sigma_u$ have been calculated from Eq. (14). Following a trend similar to that for the isotropic aggregate, continuum predictions of $\sigma_{1(0)}/\sigma_u$ lie between the upper- and lower-

TABLE III

COMPARISON OF AGGREGATE-THEORY AND HILL-CONTINUUM-THEORY YIELD-LOCI PREDICTIONS

Material	Measured r-Values	Upper-bound Aggregate Theory		Lower-bound Aggregate Theory		Hill Continuum Theory
		r-Value Prediction	$\sigma_{l(0)}/\sigma_u$ Prediction	r-Value Prediction	$\sigma_{l(0)}/\sigma_u$ Prediction	$\sigma_{l(0)}/\sigma_u$ [Eq. (14)] (Based on measured r's)
Isotropic Aggregate		1.00	1.119	1.00	1.163	1.155
Enameling Iron (composite sample)						
0° to R.D.	0.90	0.85	1.092	1.12	1.189	1.145
90° to R.D.	1.00	1.03	1.108	1.00	1.180	1.145
Aluminum-killed Steel (composite sample)						
0° to R.D.	1.92	2.64	1.200	1.99	1.257	1.339
90° to R.D.	2.06	2.33	1.204	1.84	1.240	1.339
Aluminum-killed Steel (midplane sample)						
0° to R.D.	1.92	2.20	1.172	1.85	1.244	1.339
90° to R.D.	2.06	2.08	1.187	1.75	1.240	1.339

bound aggregate-theory predictions for enameling iron. On the other hand, continuum predictions exceed both aggregate predictions for all the aluminum-killed steel data. Even though no measurements of $\sigma_{1(0)}/\sigma_u$ were made for the sample materials, the validity of the aggregate as well as continuum plasticity theories can be judged by comparison with data in the literature.

The predictions of aggregate theory and Hill's continuum plasticity theory are strictly applicable only for the description of the initial yielding of materials. However, it will be assumed, as it usually is, that these theories may be used to compare plastic flow along different strain paths if the net plastic work put in is identical.[30] In this way theoretical predictions can be compared to experimental measurements at finite strains as opposed to yielding data at the microstrain level which are difficult to obtain.

Semiatin's data[31] for a *hot-rolled* aluminum-killed low-carbon steel will be compared with the enameling iron predictions. For this material, plane strain compression[32] and uniaxial tension data were obtained for samples cut along the transverse direction of the rolled sheet. Assuming that plastic flow is not influenced by hydrostatic pressure, plane strain compression data should be the same as plane strain tension data.[20] Although r-values were measured only along the transverse direction ($r_{90°} = 0.91$), the additional r-value along the rolling direction needed to apply Eq. (14) was taken as 0.88. This value was chosen from a set of data typical for this material ($r_{0°} = 0.88$, $r_{45°} = 0.95$, $r_{90°} = 0.92$)[33]. Figure 8 is a plot of the transverse direction $\sigma_{1(0)}/\sigma_u$ for the hot-rolled aluminum-killed steel. This ratio has been taken at equal levels of plastic work, which is just the area under the uniaxial stress- or plane strain stress-plastic strain curve in these cases. Another abscissa has been plotted as well to show the level of uniaxial strain which corresponds to a given amount of work. At levels of plastic work/unit volume of 2-5 MPa (0.01-0.02 tensile strain), the measured $\sigma_{1(0)}/\sigma_u$ lies below the Hill prediction by about 7%. The upper-bound yield locus prediction (Table III) for enameling iron, a material whose texture and r-values are similar to those of the hot-rolled aluminum-killed steel, would appear to follow the small-strain behavior of this material. Certainly this behavior more closely follows the upper-bound model as opposed to the lower-bound model for which $\sigma_{1(0)}/\sigma_u$ predictions exceed the Hill prediction.

At higher tensile strains ($\varepsilon > 0.07$), the $\sigma_{1(0)}/\sigma_u$ ratio for the hot-rolled aluminum-killed steel exceeds the Hill prediction. A plausible hypothesis is that unequal hardening on the different slip systems which are activated to enforce isostrain deformation reaches such a level that only the most highly sheared systems can remain active (in both uniaxial tension and plane strain). At these strains, a single slip mode of deformation may occur,[34] and the isostress, or lower-bound, yield locus would more closely describe the deformation process. The fact remains, however, that the measurement of r's, quantities characteristic of the plastic deformation over a large strain range, for the weakly-textured enameling iron

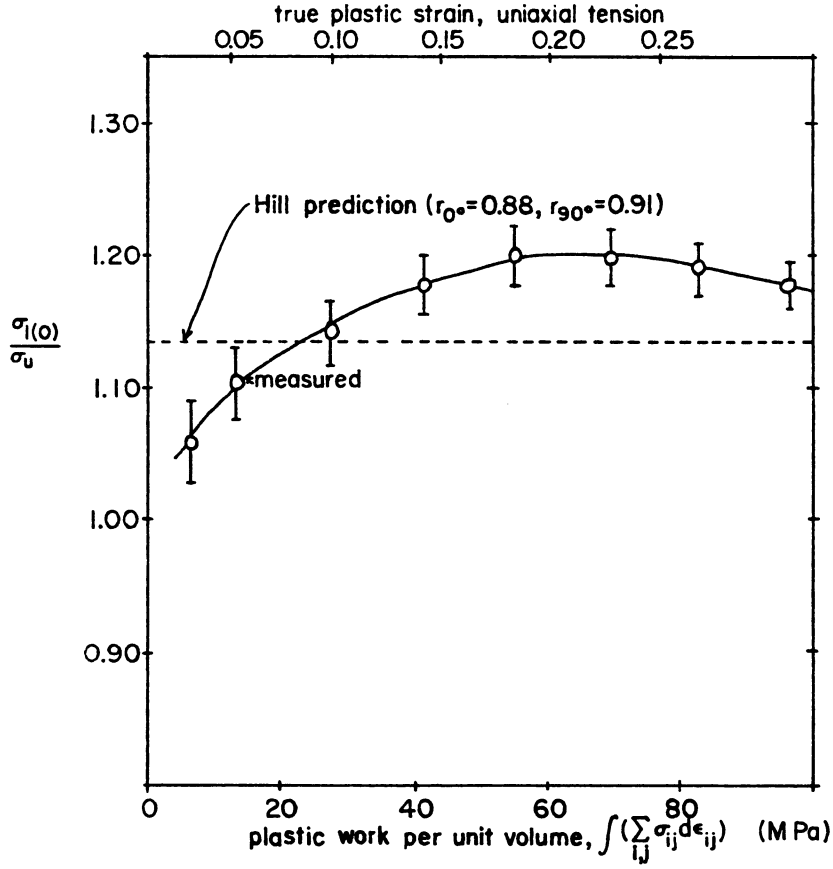

Figure 8. Ratio of plane-strain flow stress, $\sigma_{1(0)}$, to uniaxial flow stress, σ_u, for an aluminum-killed, hot-rolled low-carbon sheet steel.[31] (properties measured for T.D.)

agree more closely with upper bound, or isostrain, predictions (Figure 4).

Piehler's data for a cold-rolled, annealed aluminum-killed low-carbon sheet steel[35] can also be interpreted in terms of the predictions contained in Table III. In this case, in addition to uniaxial-tension measurements, both plane-strain tension and plane-strain compression tests were performed, the two giving similar results. This aluminum-killed steel had r-values ($r_{0°}$ = 1.83, $r_{90°}$ = 1.81) similar to those of the aluminum-killed steel described previously. Plots of Piehler's $\sigma_{1(0)}/\sigma_u$ data, for the rolling and transverse directions, are reproduced in Figures 9a and 9b. These data, which were measured only at small strains, show a Hill estimate of $\sigma_{1(0)}/\sigma_u$ to be high by about 1-5%. After examining the aluminum-killed steel data in Table III, it appears that this behavior is better characterized by a lower-bound model than an upper-bound model. The applicability of the lower-bound model here is similar to the reported findings (Figure

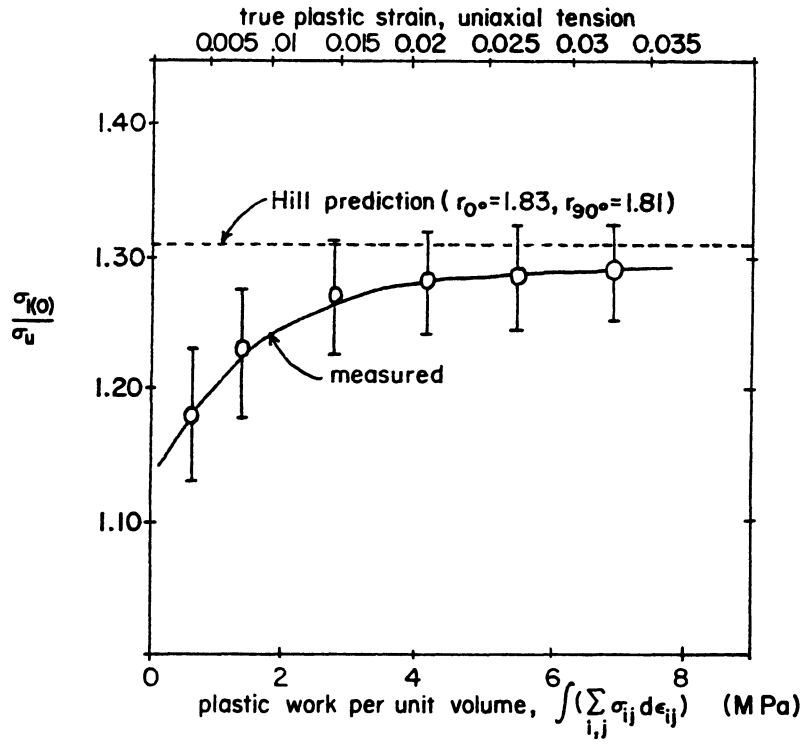

Figure 9a. Ratio of plane-strain flow stress, $\sigma_{1(0)}$, to uniaxial flow stress, σ_u, for a cold-rolled, annealed, aluminum-killed, low-carbon sheet steel.[35] (properties measured for R.D.)

5) for r-value predictions for this relatively highly-textured material.

CONCLUSIONS

The plastic deformation of BCC polycrystalline aggregates has been modeled using both an upper-bound (isostrain) approach and a lower-bound (isostress) approach. Comparison of aggregate theory and continuum-plasticity theory predictions with measured data for low-carbon steels has led to the following conclusions:

1. The initial plastic deformation of weakly-textured steels, such as enameling iron and hot-rolled low-carbon steels, is best described by an aggregate-theory yield locus derived from an upper-bound analysis. Measured r-values and the ratio of plane-strain flow stress, $\sigma_{1(0)}$, to uniaxial flow stress, σ_u, at small plastic strains support this finding. However, at higher strains, even though the r-value may remain constant, the plastic flow of these materials appears to be better described by a lower-bound analysis. This is thought to be due to latent hardening.

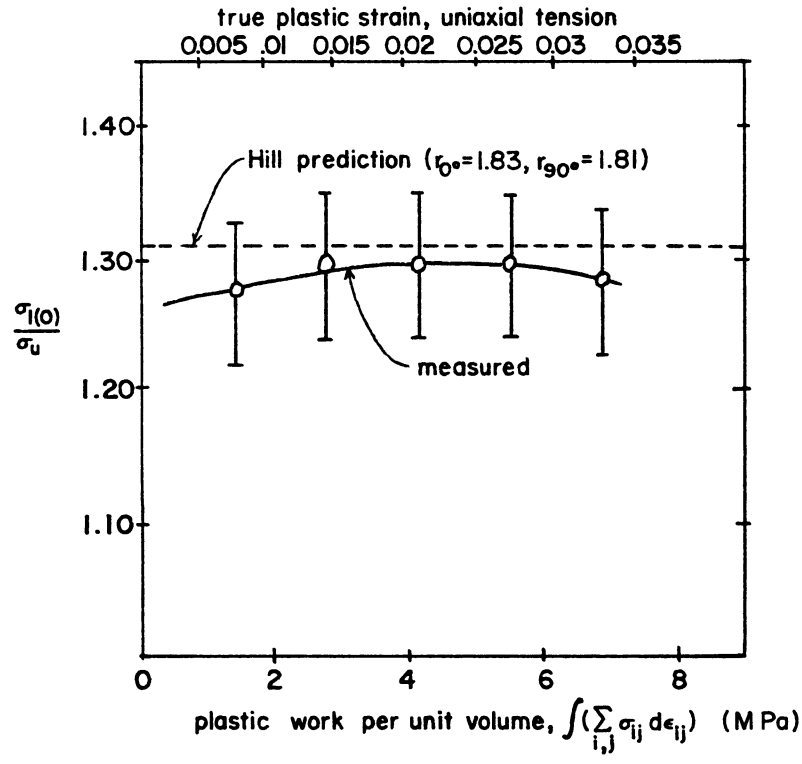

Figure 9b. Ratio of plane-strain flow stress, $\sigma_{1(0)}$, to uniaxial flow stress, σ_u, for a cold-rolled, annealed, aluminum-killed, low-carbon sheet steel.[35] (properties measured for T.D.)

2. The plastic deformation of highly-textured low-carbon steels such as cold-rolled, annealed aluminum-killed steel, appears to be better modeled by a lower-bound approach as opposed to an upper-bound approach. This conclusion is supported by the good agreement between measured values and lower-bound theoretical predictions for both r-values and flow-stress ratios $\sigma_{1(0)}/\sigma_u$.

3. In the case of the interstitial-free steel, measured r-values could not be satisfactorily accounted for by either upper- or lower-bound predictions.

4. The applicability of the upper- or lower-bound analyses for the prediction of r-values and yield loci appears to depend to a large extent on the degree of microtexture, i.e., the presence of crystallites which are likely to have nearest neighbors of similar orientation. Rimmed steels, such as enameling iron, whose r-values are of the order of 1.0 exhibit weak microtextures. In contrast, low-carbon steels with high r-values (1.6-2.0), such as cold-rolled, annealed aluminum-killed steel and interstitial-free steel, are probably more highly microtextured, as can be inferred on the basis

of their crystallite orientation distributions. In the light of the results of this investigation, the choice of upper- or lower-bound aggregate-theory models, as well as continuum theory, should be applied for the description of plastic deformation with caution.

ACKNOWLEDGMENTS

The authors would like to express their appreciation to the management of Armco Inc. for permission to publish these results. The able assistance of personnel in the Armco Research Computer Science Group, especially Mrs. Ora Thompson, is gratefully acknowledged. The support of the American Iron and Steel Institute is also acknowledged by HRP.

REFERENCES

1. W. Boas and M. E. Hargreaves, *Proc. Roy. Soc.*, 193A, 89-97 (1948).
2. G. Sachs, *Z. Ver. Deut. Ing.*, 72, 734-736 (1928).
3. G. I. Taylor, *Stephen Timoshenko 60th Anniversary Volume*, (Macmillan, New York, 1938), pp. 218-234.
4. J. F. W. Bishop and R. Hill, *Phil. Mag.*, 42, 1298-1307 (1951).
5. H. R. Piehler and W. A. Backofen, *Met. Trans.*, 2, 249-255 (1971).
6. P. R. Morris and S. L. Semiatin, *Texture Cryst. Sol.*, 3, 113-126 (1979).
7. G. Y. Chin, in *Textures in Research and Practice*, J. Grewen and G. Wassermann, eds. (Springer-Verlag, Berlin, 1969), pp. 51-80.
8. D. Thornburg, Ph.D. Thesis, Carnegie-Mellon University, Department of Metallurgy and Materials Science, Pittsburgh, Pennsylvania (1971).
9. J. W. Hutchinson, *J. Mech. Phys. Sol.*, 12, 25-33 (1964).
10. H. J. Bunge, *Z. Metallkunde*, 56, 872-874 (1965).
11. R. J. Roe, *J. Appl. Phys.*, 36, 2024-2031 (1965).
12. R. J. Roe, *J. Appl. Phys.*, 37, 2069-2072 (1966).
13. P. R. Morris and A. J. Heckler, *Advances in X-Ray Analysis*, 11, 454-471 (1968).
14. I. L. Dillamore and H. Katoh, *Metal Science*, 8, 21-27 (1974).
15. G. I. Taylor, *Proc. Colloq. on Deformation and Flow of Solids*, Madrid, 1955, (Springer-Verlag, Berlin, 1956), pp. 3-12.
16. P. Parnière and L. Roesch, *Mem. Sci. Rev. Mét.*, 72, No. 3, 221-240 (1975).
17. M. Grumbach, P. Parnière, L. Roesch, and C. Sauzay, *Mem. Sci. Rev. Mét.*, 72, No. 3, 241-253 (1975).
18. G. I. Taylor, *Proc. Roy. Soc.*, 107A, 337-361 (1926).
19. H. R. Piehler and W. A. Backofen, in *Textures in Research and Practice*, J. Grewen and G. Wassermann, eds., (Springer-Verlag, Berlin, 1969), pp. 436-443.
20. W. A. Backofen, *Deformation Processing*, (Addison-Wesley, Reading, Mass., 1972).

21. D. C. Drucker, in *Proc. First U.S. Nat. Cong. Appl. Mech.*, 1951, pp. 487-491.
22. W. F. Hosford and W. A. Backofen, in *Fundamentals of Deformation Processing*, (Syracuse University Press, Syracuse, New York, 1964), pp. 259-298.
23. S. L. Lopata and E. B. Kula, *Trans. AIME*, 224, 865-866 (1962).
24. R. E. Hook, A. J. Heckler, and J. A. Elias, *Met. Trans.*, 6A, 1683-1692 (1975).
25. A. J. Heckler and W. G. Granzow, *Met. Trans.*, 1, 2089-2094 (1970).
26. P. O. Metz, Ph.D. Thesis, Carnegie-Mellon University, Department of Metallurgy and Materials Science, Pittsburgh, Pennsylvania (1975).
27. R. Hill, *The Mathematical Theory of Plasticity*, (Clarendon Press, Oxford, 1950), Ch. XII.
28. W. Johnson and P. B. Mellor, *Engineering Plasticity*, (Van Nostrand, London, 1973).
29. W. A. Backofen, W. F. Hosford, and J. J. Burke, *Trans. ASM*, 55, 264-267 (1962).
30. G. N. White and D. C. Drucker, *J. Appl. Phys.*, 21, 1013-1021 (1950).
31. S. L. Semiatin, Ph.D. Thesis, Carnegie-Mellon University, Department of Metallurgy and Materials Science, Pittsburgh, Pennsylvania (1977).
32. H. Ford, *Proc. Inst. Mech. Engrs.*, 159, 115-143 (1948).
33. R. Hook, Unpublished research, Armco Inc., Middletown, Ohio.
34. F. Ronde-Oustau and B. Baudelet, *Acta Met.*, 25, 1523-1529 (1977).
35. H. R. Piehler, Sc.D. Thesis, MIT, Department of Metallurgy and Materials Science, Cambridge, Mass. (1967).